

Micro Urban Electric Vehicle Phase II – Modeling

Final Report

Bradley University
Department of Electrical and Computer Engineering
12 May 2010

Students:

Brian Kuhn
Steven Komperda
Matthew Leuschke

Advisors:

Dr. Huggins
Dr. Anakwa
Mr. Gutschlag

Abstract

The goal of the MUEV project is to create a commercially viable, low carbon-footprint electric vehicle capable of being used on a typical daily commute. The goal of Phase I was to purchase the components of the vehicle, assemble it, and test its regenerative capabilities. The goal of the Phase II design project is to create an accurate model of the electric vehicle in Simulink© to be used by the Phase III design project, who will optimize the vehicle. The model consists of each of the major components of the vehicle, which include the battery, the motor, the controller, and the vehicle dynamics. The Simulink© simulation results are within 10% of the experimental vehicle test results.

Table of Contents

I.	Introduction.....	1
II.	System Identification and High Level Design.....	1
	A. High Level Physical Diagram.....	1
	B. Modeling.....	2
	1. High Level Simulink© Block Diagram.....	3
	2. Simulation Requirements.....	4
III.	Detailed Modeling.....	4
	A. Motor Model.....	4
	1. Test Procedure.....	5
	2. Model Development.....	6
	3. Test Results.....	8
	B. Controller Model.....	11
	1. Test Procedure.....	12
	2. Model Development.....	15
	3. Test Results.....	16
	C. Vehicle Dynamics Model.....	18
	1. Model Development.....	18
	2. Test Results.....	20
	D. Battery Model.....	21
	1. Model Development.....	21
	2. Battery Model Results.....	23
	E. Complete System.....	24
IV.	Conclusion.....	24
V.	Recommendations for Future Work.....	25
VI.	Patents.....	26
VII.	Standards.....	27
VIII.	References.....	29
IX.	Appendix A.....	30
X.	Appendix B.....	36
XI.	Appendix C.....	37

I. Introduction

It is well known that there is a finite supply of hydrocarbon based fossil fuels and that, ultimately, modern economies have to find renewable sources of energy. Alternative energy sources and enhanced energy efficiency are among the leading technical challenges in implementing this change. The Electrical and Computer Engineering Department at Bradley University has decided to participate in meeting these challenges and has launched a multi-year project that aims to develop a commercially viable low carbon footprint electric vehicle for urban commuting. This requires an ultra compact, lightweight vehicle that is also street legal. It will be capable of holding two passengers, traveling up to 55 mph, and traveling up to 50 miles in all weather conditions, making it ideal for a daily commute for the average user [1].

In the first phase of this project, the team performed research in order to design and implement a prototype test platform for a low carbon footprint, single passenger urban electric vehicle. In order to accomplish this, the team researched available battery technology, motors, electronics, and design concepts for regenerative braking. While the previous team addressed some of the issues surrounding the mechanical design, the detailed design of all the vehicle subsystems, particularly regenerative braking and optimized battery sizing, is the next major step in development. In order for this to be implemented, detailed models for vehicle subsystems must be developed.

II. System Identification and High Level Design

In the 2009-2010 academic year, the project entered its second phase. Using the research, design and test platform developed by the phase I team, this year's team has created a Simulink© system block diagram that models the vehicle subsystems and vehicle dynamics.

A. High Level Physical Diagram

Figure 1 shows the high-level block diagram of the physical experimental platform. The user (driver) controls the throttle and brake. The throttle is transformed into an electrical input to the controller and the brake is transformed into a disturbance. Based on the throttle input, the controller develops two PWM signals from the battery terminal

voltage. These signals are applied to the field and armature windings of the motor with duty cycles adjusted for desired motor speed and torque. When the shaft torque is applied to the rear axle the vehicle dynamics (speed and acceleration) changes depending on the vehicle properties such as vehicle mass, wheel friction, and wheel inertia. The data acquisition is used to verify the signals and parameters of the subsystems as well as the vehicle dynamics.

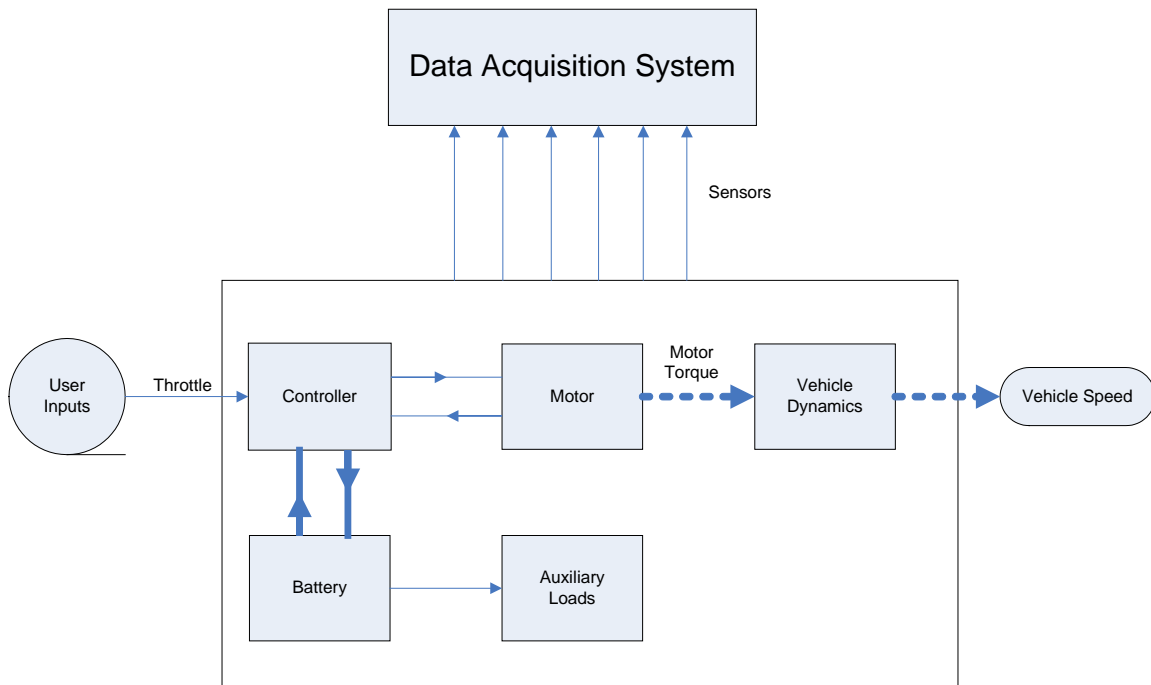


Figure 1: High Level Block Diagram of Experimental Platform

B. Modeling

For the motor, battery, and vehicle dynamics, the team first developed an analytical model, made experimental measurements, and then finalized the model. In the case of the controller an empirical approach was used due to the fact that no data was available relating the inputs and outputs of the controller. Therefore, the controller needed to be tested experimentally in various conditions. The initial goal to begin the modeling process was to acquire the necessary experimental data to not only develop the Simulink© blocks, but also to test their validity. Using this data, the team developed each individual Simulink© block of the platform and tested the outputs given by the

simulation against the experimental results. Through iteration the model was refined. This project provides the future design teams with an accurate and flexible Simulink© model for vehicle design. The ultimate goals for this phase are as follows:

- Modeling
 - DC Motor
 - Controller
 - Vehicle Dynamics
 - Battery
- Verify and Optimize Model
 - Perform data acquisition and compare with experimental results of current platforms
 - Adjust model until desired performance is achieved.
 - Compare experimental and simulated outputs of subsystems and modify Simulink© blocks as necessary
 - Optimize Simulink© blocks

1. High Level Simulink© Block Diagram

Figure 2 shows the high-level overview of the Simulink© block diagram model for the current physical platform. The inputs are throttle and brake, which are derived from measured driving data obtained from the data acquisition system on the physical platform.

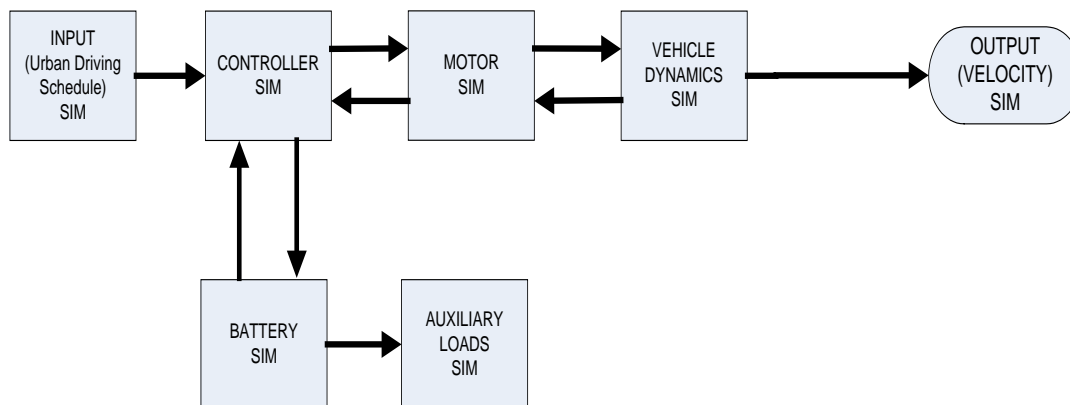


Figure 2: Simulink© High Level Block Diagram

The controller block accepts the battery terminal voltage from the battery block and the throttle signal input generates two PWM signals applied to the motor block. This PWM signal provides the input to the motor block, generating motor torque and back EMF. The vehicle block accepts the motor torque and applies it to the vehicle properties, which include vehicle weight, vehicle inertia, aerodynamic forces, and rolling resistances to produce the velocity of the vehicle. The auxiliary load block consists of heat, A/C, lights, and radio and draws current from the battery whenever in use.

The regenerative braking feature of the MUEV occurs when there is a zero throttle input. The vehicle speed will be fed back through a parallel path of the motor model, which serves as a generator. This then feeds back to a parallel controller block, which is the same physical controller block but behaves differently for regenerative current.

2. Simulation Requirements

Each simulation block needs to be capable of producing 10 percent accurate outputs given reasonable user inputs and accurate system block parameters. Each system block shown in Figure 2 has specific parameters that can be adjusted for replacement components.

III. Detailed Modeling

A. Motor Model

The motor used is a separately excited 24-48 volt DC motor, manufactured by D&D motors, with a peak rating of 17 HP and 8 HP continuous. A separately excited motor makes use of two internal windings: an armature and a field. Each winding has a separate voltage input that can be varied to optimize the needed torque or speed output of the motor. Figure 4 describes the generic setup of the motor testing arrangement used to measure the motor characteristics. The voltages were measured using voltmeters and oscilloscopes, while ammeters were used in series with the armature and field windings, to measure currents.

1. Test Procedure

The armature resistance (R_a) is the most difficult parameter to accurately measure. This is because it is dependent on the armature current (I_a), and high current tests had to be performed in order to acquire the proper range of variance in R_a . Initially, a locked-rotor test was performed by reducing the field voltage and using Ohm's Law on the armature. The results indicated that if $R_a = V_a / I_a$, then $1.26V / 15.5A = 0.081$ ohms. However, this test lacked a means of verifying R_a 's value in relation to I_a , so a more rigorous test over a wide range of armature currents was conducted. By lowering the field current to nearly zero and measuring R_a at different values of I_a , a more accurate scale of R_a was made. Additional tests were made using power resistors to provide a range of R_a values over very high currents. The final range of R_a is shown in Table 1, shown below.

Table 1: R_a vs. I_a Measurements

Ra Measurement Scale		
Armature Voltage (V)	Armature Current (A)	Armature Resistance (Ohms)
1.24	20.6	0.060194175
1.575	30	0.0525
1.86	40	0.0465
2.3	60	0.038333333
2.65	70	0.037857143
2.8	80	0.035
3.05	90	0.033888889
3.35	100	0.0335
4	147	0.027210884
4.2	160	0.02625

The measurement of the field resistance (R_f), was much simpler than R_a since the field resistance of the motor is independent of current. Ohm's Law gives the relationship of $R_f = V_f / I_f = 1.35$ ohms.

The rest of the parameters required transient tests to be made on the motor. Plots of these tests can be found in Appendix B. Finding the armature inductance (L_a) and field inductance (L_f) required reading the behavior of V_a and V_f as the motor turned on. The curve displayed by the behavior of these voltages provided a time constant for the respective inductance, which could then be solved by multiplying by its respective resistance. The value for L_f is therefore shown as $L_f = R_f * \tau_f = 0.396$ H. While the time

constant for τ_a was found to be 2.4 ms, L_a changes as a function of R_a , which is a function of R_a . Therefore, it is displayed in the motor model by being the product of τ_a and R_a inverted, where R_a has a lookup table to correspond with Table 1.

Recording the motor inertia (J) involved an opposing method to the inductance tests. Instead of using a start-up test, J was solved using a coast-down test. Taking the motor to a steady state, shutting it down, and then seeing the transient behavior of V_a allowed for the time constant of J to be recorded. To find J, the viscous friction “b” had to be found. In order to solve for b, it must be acknowledged that

$$\Sigma \text{torques} = T_d - T_{CF} - b\omega_s = K_T I_a - T_{CF} - b\omega_s = 0 \quad (1)$$

By using equation 1 at different speeds, and combining with equation 2, two sets of speed data can be taken, one to solve for T_{CF} and one for b.

$$K_T = K_m I_f = 1.16 * 10^{-4} I_f^3 - 0.00396 I_f^2 - 0.0455 I_f \quad (2)$$

Using this method, $T_{CF} = 0.746694$ [N*m] and $b = 0.00589$. Having b allows for the use of the following equation

$$V(t) = v_o * e^{(-t/\tau_J)} = v_o * e^{(-b/J)*t} \quad (3)$$

where $v_o = 20.3$ V. Solving for J yields $J = 8.2 * 10^{-5}$ [kg*m²].

2. Model Development

Based on the measurements described in subsection 2, a Simulink© model was developed and is shown in Figure 3. The motor accepts two PWM signals from the controller and generates a field and armature current to control the shaft velocity [2]. The field current i_f is described as

$$V_f = R_f i_f + L_f (di_f/dt) \quad (4)$$

The armature current can be found from solving equation 5.

$$V_a = R_a I_a + L_a (dI_a/dt) + E_g \quad (5)$$

The motor back emf is expressed in equation 6.

$$E_g = K_v \omega i_f \quad (6)$$

The torque developed by the motor is seen in equation 7.

$$T_d = K_t i_f i_a = J(d\omega/dt) + B\omega + T_L \quad (7)$$

Where ω = motor speed [rad/s]

B = viscous friction constant [N*m/rad/s]

K_v = voltage constant [V/A * rad/s]

$K_t = K_v$ = torque constant

L_a = armature circuit inductance [H]

L_f = field circuit inductance [H]

R_a = armature circuit resistance [ohms]

R_f = field circuit resistance [ohms]

T_L = load torque [N*m]

Originally, the torque would then pass through a mechanical transfer function, which incorporated the viscous friction coefficient of the motor b and the inertia of the shaft J , in order to output a shaft velocity. However, while this configuration works with traditional motor models, the model had to be adjusted to interact with the vehicle dynamics. It is desired for the inertia created by the vehicle mass, as well as that of the wheels, to be referred back to a single point in the model. To do this, the transfer function block for the mechanical side of the motor cannot be used, since Simulink© does not let

variables be used as inputs to its transfer function block. Thus, the motor model now outputs a developed torque of the motor to drive the vehicle dynamics, which will be explained later in this document. The final model of the motor is shown in Figure 3 below.

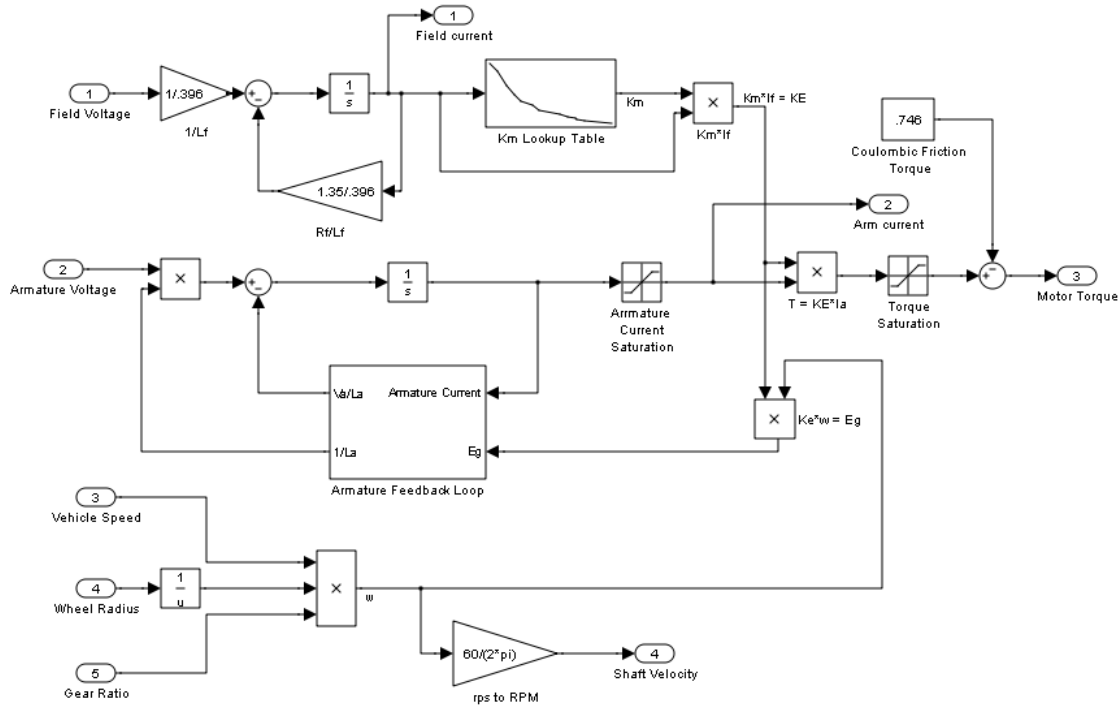


Figure 3: Simulink© Motor Model

3. Test Results

In order to test the motor model the field and armature were connected to a variable voltage supply as seen in figure 4. The current in the armature and field windings were measured and the voltage measurements were taken using the Data Acquisition System (DAQ), which is referenced in appendix A.

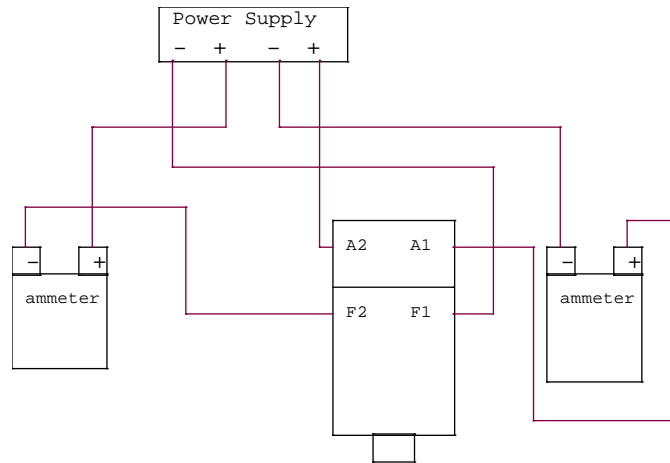


Figure 4: Circuit Diagram for Motor Tests

To test the results, voltages recorded from the no-load data were used as inputs to drive the Simulink© model. First, shunt voltage data were compared between simulated and experimental results. This data can be seen in Table 2, with the simulated results for each voltage shown on Table 3. As indicated by these tables, the simulated results are well within the +/- 10% goal of the actual motor speed.

Table 2: Experimental Motor Testing Results

Tested				
Armature Voltage (V)	Field Voltage (V)	Armature Current (A)	Field Current (A)	Shaft Speed
4	4	7.4	3.2	350
6	6	6.5	4.6	442
8	8	6.2	6.4	532
10	10	6.2	7.9	635
12	12	6.2	9.3	728
14	14	6.4	10.4	830
16	16	6.6	11.5	960
18	18	7	12.6	1085
20	20	7.3	13.7	1187
22	22	7.6	14.6	1292
24	24	8	15	1410
26	26	8.3	16	1513
30	30	8.9	17.4	1717

Table 3: Simulink© Shunt Testing Results

Simulink© Model				
Armature Voltage (V)	Field Voltage (V)	Armature Current (A)	Field Current (A)	Shaft Speed (RPM)
4	4	13.3	2.67	366
6	6	10.2	4	465
8	8	9	5.33	552
10	10	8.7	6.67	653
12	12	8.7	8	754
14	14	8.6	9.33	843
16	16	8.75	10.67	943
18	18	9.3	12	1071
20	20	9.65	13.32	1183
22	22	9.85	14.67	1282
24	24	10.13	16	1385
26	26	10.29	17.33	1477
30	30	11	20	1695

In order to confirm that the motor model was accurate over all ranges of shaft speed for the system, similar tests were run at throttle position intervals. The throttle position is acquired by connecting the motor controller to the motor, which will be explained in more detail in the next section. The circuit diagram of this setup is shown in Figure 7. The results from the test data are shown in Table 4 and the data are plotted in Figure 8.

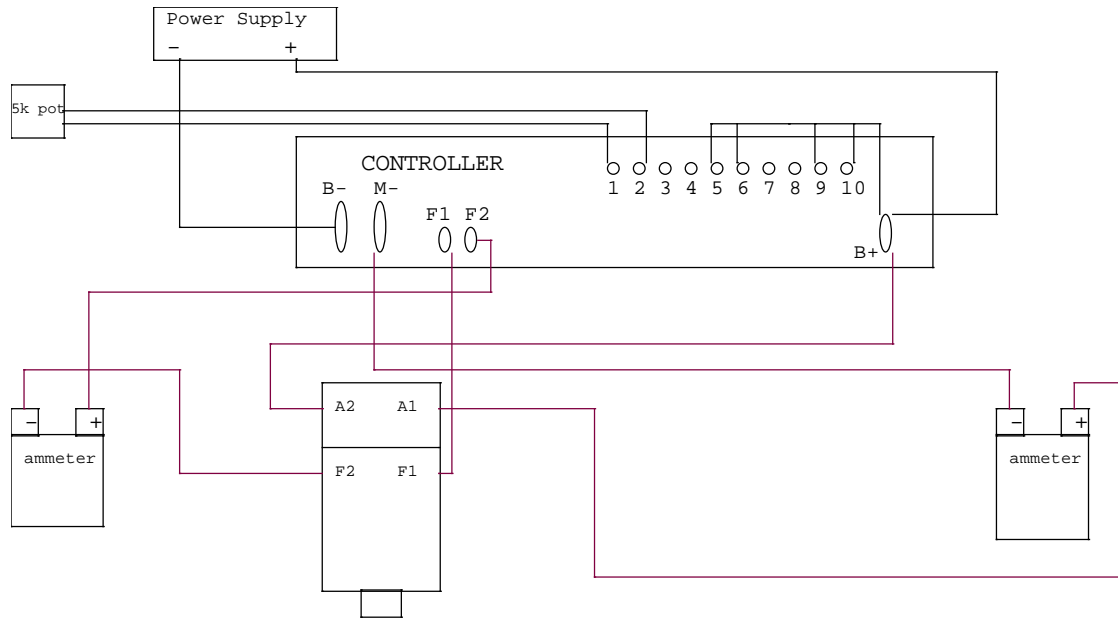


Figure 7: Circuit Diagram for Motor w/ Controller Tests

Table 4: Motor w/ Controller Testing Results

Throttle Position	Experimental Speed (RPM)	Simulated Speed
10	90	33
20	364	295
30	655	593
40	1060	915
50	1485	1360
60	2165	1900
70	3030	2870
80	3506	3344
90	4175	4000
100	4770	4555

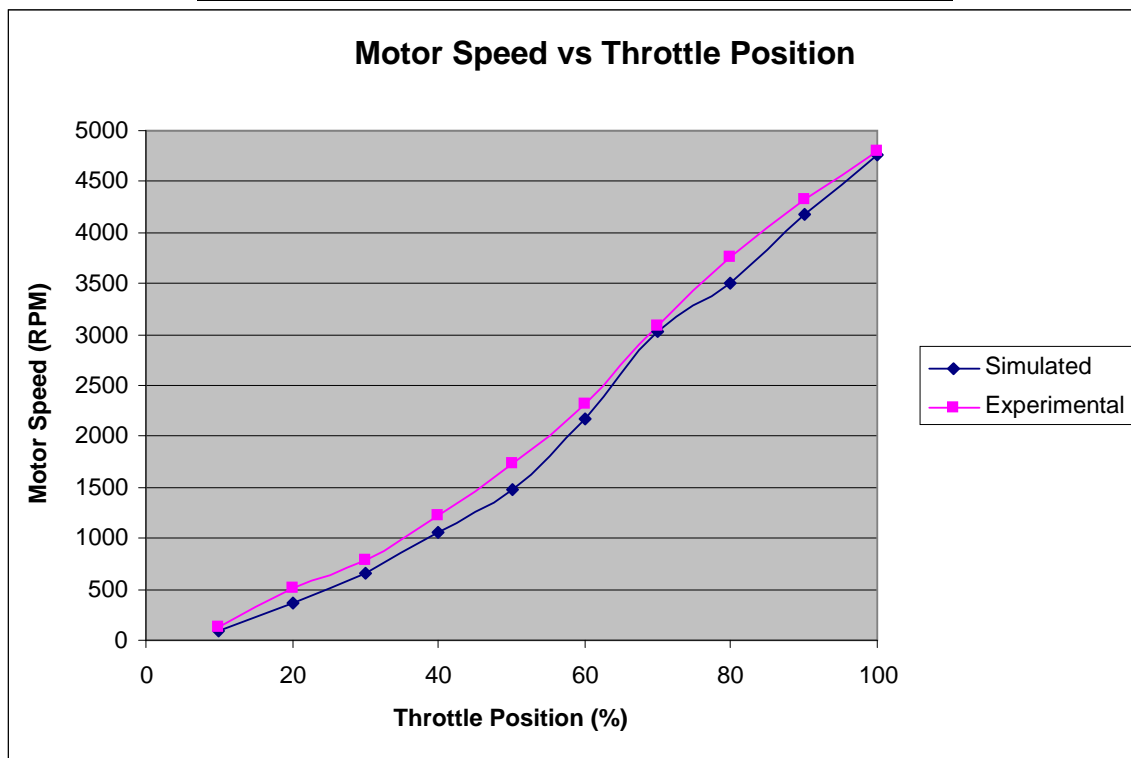


Figure 8: Experimental and Simulated Motor Results

B. Controller Model

The controller used is an Altrax DC-X 600. It develops two PWM signals at a frequency of 18 kHz and is capable of delivering 600 A to the motor for a period of 2 minutes, 350 A for 5 minutes, and 250 A for 1 hour.

1. Test Procedure

In order to test the controller, measurements of the armature and field voltages and currents had to be taken at different throttle positions. This allowed a relationship between the armature and field currents to be determined. Tests were performed with power resistors, which replaced the connection of the armature side of the motor to the batteries, to simulate loads on the battery that would be experienced when the motor is on the vehicle. Table 5 shows one of the sets of data taken from the controller with high armature currents using power resistors.

Table 5: Controller Test Data

Controller Test #2 3/11/10 10:30 A.M.								
Throttle	Battery Voltage [V]	Armature Current [A]	Field Current [A]	Armature Duty Cycle [%]	Field Duty Cycle [%]	Armature Amplitude [V]	Field Amplitude [V]	Motor Temp [F]
100	29	110	3.45	100	18.4	29.5	28.5	81.8
90	30.2	103	3.75	86.4	16	31.5	31	78.5
80	32.6	90.5	3.7	74.2	15.5	32	32	79
70	32.4	82	3.4	66	14.7	32	32	79
60	32.44	70.5	4	54.95	16.9	32	32.5	79
50	32.73	60	4.5	45.7	19.4	32.5	32.5	79
40	33.16	48	5.45	36.2	22.36	33.2	33	80
30	33.65	35	6.4	26.8	25.9	33	33.5	80
20	34.34	19.5	7.35	15.5	29.4	33.5	33.5	80
10	34.94	5.1	8.45	4.78	33.3	33.65	34.5	80
0			33		36.5			
Voc (start)	37.5							
Voc (end)	35.4							

The behavior of the field current at high armature currents suggests that there is a relationship between the two after a certain armature current. Graphing these results make the relationship even more apparent, which are shown in Figures 9 and 10.

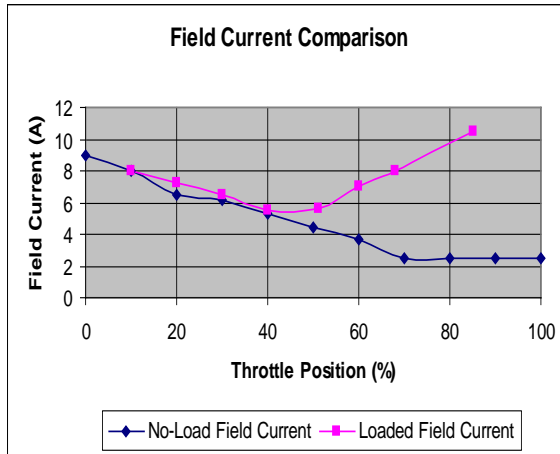


Figure 9

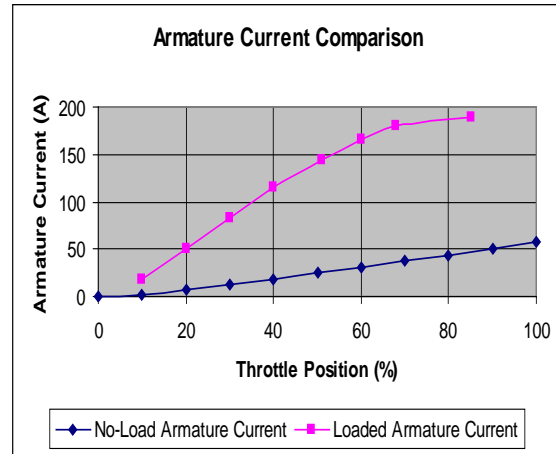


Figure 10

An improved test was needed that would allow direct control over the loads at a given throttle position. This is necessary in order to separate the relationship between the armature and field currents from the relationship between the field current and the throttle position.

In order to accurately describe the relationship between the armature current and field voltage duty cycle under known load torques, while also being able to measure the shaft speed, tests were performed on a dynamometer. The dynamometer used was built by Go-Power Corporation. A range of loads were tested at varying throttle positions to measure the output of armature current and duty cycle of the field voltage using the experimental set shown in Figure 8. In order to set up this experiment, the motor was mounted onto the dynamometer platform and the other vehicle components, including the controller, batteries, and all of the measuring equipment that had been used prior, were set up next to the dynamometer. Unfortunately, the dynamometer used for testing could not produce high load torques at low speeds due to the fact that the load forces were supplied by water pressure. This limited the ability to measure controller characteristics at low throttle positions; particularly any speeds below 2000 RPM no-load. Table 6 shows the results of the dynamometer testing.

Table 6: Dynamometer Test Results

Dynamometer Test Results							
Throttle (%)	Force (lbs)	Speed (RPM)	Armature Current	Field Current	Armature Voltage	Field Voltage	Battery Voltage
100	0.75	4840	18.63	2.28	37	2.89	36.98
100	2.25	4450	33.44	2.39	36	3	36.61
100	6.5	3810	54.11	3.01	34.7	3.36	35.52
100	10.75	3135	95.04	4.02	33.9	4.45	34.46
100	14	2760	116.32	4.74	32	5.48	33.25
100	16.25	2450	132.15	5.66	30.5	5.9	31.38
100	18.25	2115	136.7	5.95	26.5	6.4	30.77
92	0.5	4233	17	2.31	32.5	2.92	37.38
92	3	3800	38.41	2.44	31.6	3.05	36.64
92	6	3330	62.8	2.73	60.7	3.38	35.95
92	9	2930	84.49	3.59	30	3.9	35.33
92	12.5	2580	108.86	4.51	29.16	4.83	34.55
92	16	2315	130.59	5.49	28.23	5.85	33.71
83	0.56	3840	15.35	2.39	29.8	3.03	37.78
83	2.75	3415	36.6	2.52	28.8	3.15	36.84
83	6	2980	64.19	2.71	27.84	3.47	35.88
83	9.25	2625	87.19	3.46	27	4.14	35.07
83	12.25	2345	104.55	4.42	26.28	4.89	34.38
83	15	2130	121.45	5.05	25.67	5.34	33.77
62	0.55	2438	12.5	3.25	22.3	3.7	37.5
62	4.5	2192	46	3.5	21.5	3.85	36.6
62	7.5	2040	70	4	21.01	3.95	36.15
62	13.25	1714	112	4.8	20.1	5.1	34.8
55	0.5	1760	9.71	4.12	18.94	5.23	37.76
55	3	1670	29.6	4.16	18.61	5.21	37.17
55	6	1560	50.84	4.38	18.17	5.32	36.52
55	9	1460	72.64	4.95	17.72	5.46	35.92
55	9.75	1445	77.01	5.12	17.57	5.48	35.69

The test results are important because they allowed for a relationship between the field voltage duty cycle and armature currents to be established. The model is configured to use a polynomial equation to calculate the field current as a function of the armature current, which changes based on the throttle position the vehicle is set to at the time. To compensate for the lack of lower throttle position data, the lowest throttle position's equation is applied to all of the lower end throttle positions.

2. Model Development

The model for the Alltrax Separately-Excited Controller had to be created entirely from test data and the patterns observed in that data. The basic concept behind the controller is that it accepts a throttle position input from the user and translates this into two PWM signals: one for the armature voltage and one for the field voltage. These PWM signals are then multiplied by the current battery voltage to give an appropriate voltage (based off of the PWM's duty cycle) to feed to the armature and field of the motor.

Without aid from the manufacturer, it is incredibly difficult, to the point of being well outside the scope of this project, to have precise mathematical explanations as to how the armature and field voltages are reacting, both in relation to the throttle position and to each other. General knowledge of how a separately-excited DC motor is supposed to operate can give some insight on how one might design a controller to drive it. The armature winding of the motor is responsible for the speed of the shaft, while the field winding is responsible for the torque being generated at the shaft. At a standstill, the vehicle will need a larger amount of torque to overcome static friction forces and to get the motor up to a steady state speed. This would translate to a higher field voltage being applied at lower throttle positions. Once the vehicle has reached a high speed, the field voltage lowers and the armature voltage continues to climb, allowing the motor to speed up. This relationship alone would allow a simplistic controller to be designed to react only to the throttle position input.

However, a motor designed to drive any kind of significant load would need to have a mechanism in place to allow the field voltage to react to that load, allowing more torque to be called upon to drive the shaft under such loads. In the motor model, the back EMF voltage running through the armature allows the motor to react to loads, increasing the armature current to drive heavier loads. This armature current must therefore be fed back to the controller, with the thought being that the controller will respond by supplying more torque via the field winding so as to prevent having to rely wholly on the armature to drive the system, which is ultimately the point of a separately-excited system. With this behavior in mind, the controller model seen in Figure 11 was developed.

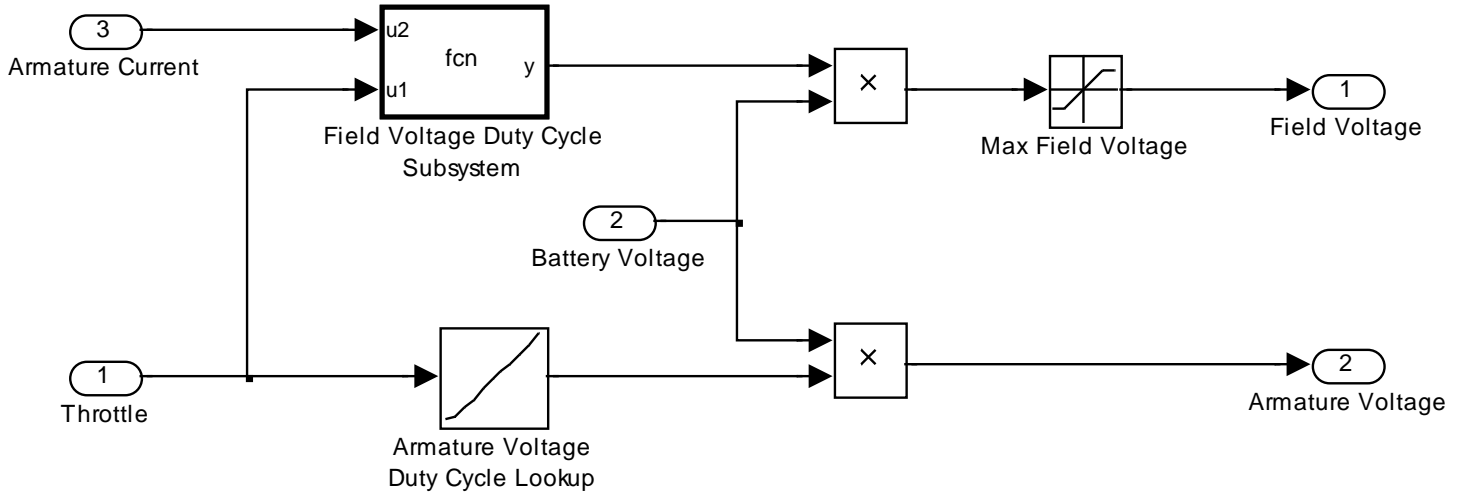


Figure 11: Simulink© Controller Model

The model accepts a throttle position, which is fed to the armature and field to create a duty cycle. This duty cycle gets multiplied by the current battery voltage in order to create the actual voltage. The armature reacts only to the throttle position based on a look-up table from the test data, while the field duty cycle is a function of the armature current. The function chosen to generate that field duty cycle is dependent on the current throttle position.

3. Test Results

The best way to test the controller was to run the simulation with just the controller and motor models and having a step input to represent the throttle position. This information was already shown in Figure 8 and Table 4. The simulated plot matches up very closely with the experimental plot for RPM vs. throttle position.

The other aspect of the controller model that had to be verified was whether or not the voltages were behaving correctly. A scope plot of the voltages being fed to the motor at 80% throttle position is shown in Figure 12.

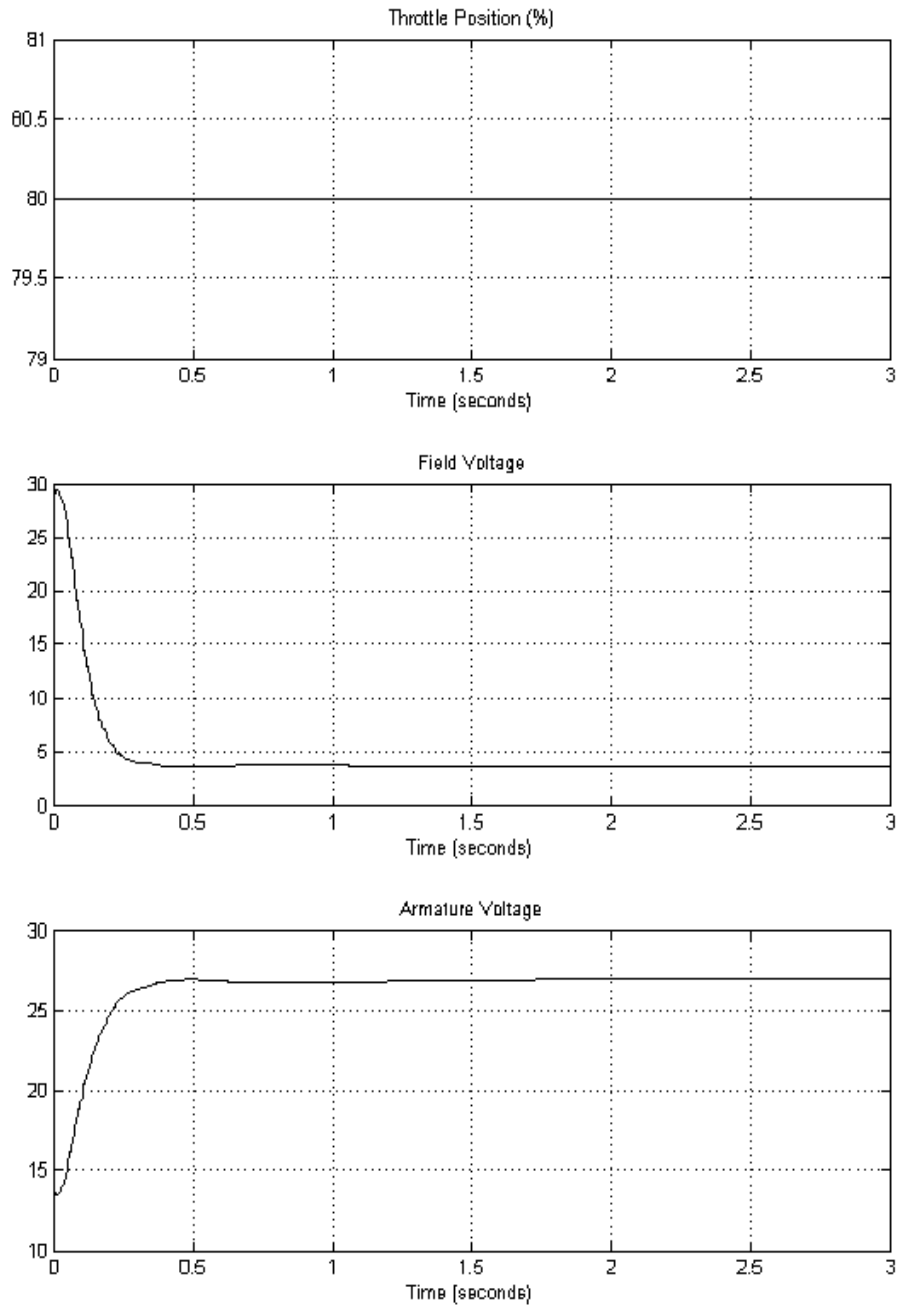


Figure 12: Controller Voltage Behavior

As expected of separately excited DC controller behavior, the controller starts by outputting a higher field voltage to create more torque to in the system, enabling the vehicle to overcome static friction forces. The field then decreases while the armature voltage rises to allow the shaft to rotate faster.

C. Vehicle Dynamics Model [3][4]

The vehicle dynamics consists of an American SportWorks Vector Go Kart frame. It is capable of mounting all of the components purchased and has a total carrying capacity of 310 lbs.

1. Model Development

The vehicle dynamics model for the MUEV is designed to incorporate the properties of the chassis and accept input parameters such as passenger mass and grade in order to accurately account for the load imposed on the system. In doing so, the speed of the vehicle is generated. In order to obtain a vehicle speed that incorporates the forces generated by the motor working against aerodynamic forces, rolling resistance forces, and static frictional forces, a relationship between all of these forces must be developed.

If the entire system is referred back to the wheels, a torque relationship can be established, as shown below.

$$T_w = F_x r_w + J_{tot} \dot{\omega}_w + B_{tot} \omega_w + T_{SFtot} \quad (8)$$

Where T_w = torque at the wheel and axel

F_x = tractive force at the wheel

r_w = wheel radius

J_{tot} = motor + wheel inertia

ω_w = wheel angular speed

$\dot{\omega}_w$ = wheel angular acceleration

B_{tot} = motor + wheel viscous friction coefficient

T_{SFtot} = total static frictional torque

Equation 8 can be adjusted to become a function of the tractive force.

$$F_x r_w = T_w - J_{tot} \dot{\omega}_w - B_{tot} \omega_w - T_{SFtot} \quad (9)$$

$$F_x = T_w / r_w - J_{tot} \dot{\omega}_w / r_w - B_{tot} \omega_w / r_w - T_{SFtot} / r_w \quad (10)$$

Since $v_x = \omega_w * r_w$ where $\omega_w = v_x / r_w$ and $\dot{\omega}_w = a_x / r_w$ then equation 11 results.

$$\dot{\omega}_w / r_w = \dot{v}_x / (r_w)^2 = a_x / (r_w)^2 \quad (11)$$

Here, $\dot{v}_x = a_x$, which equals the linear acceleration of the vehicle. Now, let $J_{tot} = J_m N^2 + J_w$, where J_m = inertia of the motor shaft, J_w = inertia at the wheels, and $N = n_{wheel} / n_{motor}$ = gear ratio. Equation 10 can be rewritten to become the following.

$$F_x = T_m * N / r_w - [J_m N^2 + J_w] * \dot{v}_x / (r_w)^2 - B_{tot} v_x / (r_w)^2 - T_{SF_{tot}} / r_w \quad (12)$$

By considering $B_{tot} v_x / (r_w)^2 + T_{SF_{tot}} / r_w$ to be an inefficiency in generating T_w , η can be substituted where $\eta \approx 0.8$ to 0.9 . This can then be written as the following.

$$F_x = T_m * N * \eta / r_w - [J_m N^2 + J_w] * \dot{v}_x / (r_w)^2 \quad (13)$$

Next the masses of the vehicle and passenger must be considered, as well as the rolling resistance, aerodynamic, and grade forces. To relate total force of the vehicle to F_x and the forces working against F_x , the following is established.

$$M * a_x = F_x - R_x - D_A - M * g * \sin(\theta) \quad (14)$$

Where M = mass of the vehicle and its passengers

R_x = rolling resistance forces

D_A = aerodynamic forces

$M * g * \sin(\theta)$ = force due to grade of road

Then, substituting in for F_x , a relationship for the vehicle acceleration can be established.

$$M * a_x = T_m * N * \eta / r_w - [J_m N^2 + J_w] * a_x / (r_w)^2 - R_x - D_A - M * g * \sin(\theta)$$

$$[M + (J_m N^2 + J_w) / (r_w)^2] * a_x = T_m * N * \eta / r_w - R_x - D_A - M * g * \sin(\theta) \quad (15)$$

Letting $K = M + (J_m N^2 + J_w)/(r_w)^2$, equation 15 can be simplified into a clear expression of vehicle acceleration.

$$a_x = \dot{v}_x = T_m * N * \eta / (K * r_w) - R_x / K - D_A / K - M * g * \sin(\theta) / K \quad (16)$$

A final integration of \dot{v}_x gives the vehicle velocity v_x . The model shown in Figure 13 incorporates the above equations to give the simulated vehicle velocity. The models of the subsystems for the vehicle dynamics can be seen in Appendix B.

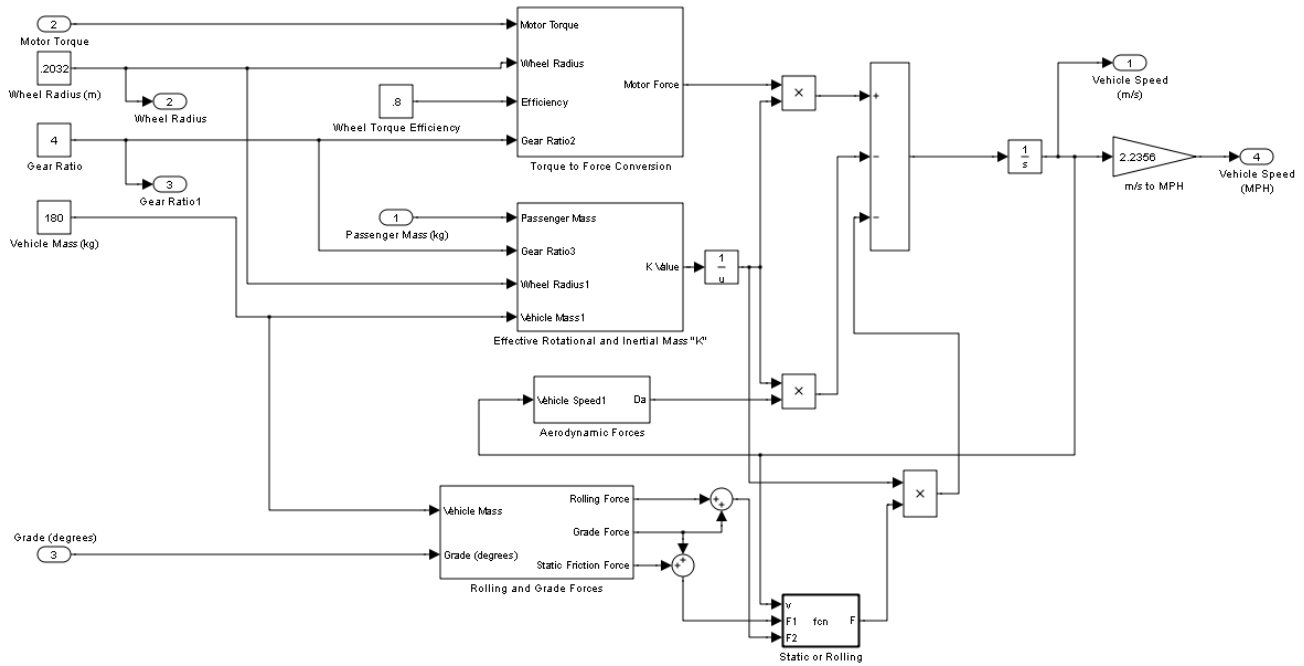


Figure 13: Simulink© Vehicle Dynamics Model

2. Test Results

First, the mass of the chassis was estimated from a combination of the manufacturer specifications of the batteries, motor, and frame, minus the gasoline engine that originally would have been mounted on the frame. Using the equation for rolling resistance seen in equation 17, the coefficient of rolling resistance was estimated by using the coefficient of rubber tires on concrete.

$$R_x = C_{rr} N_f \quad (17)$$

The coefficient of static friction was measured by using a force gauge to determine the amount of force that was needed to initially start the vehicle moving. Finally, using the equation for aerodynamic drag, seen in equation 18, the coefficient of drag coefficient (C_d) was estimated by using similar drag coefficients from vehicles of similar shapes.

$$D_a = 1/2 * \rho v^2 C_d A \quad (18)$$

Ideally, each parameter of the vehicle dynamics would be measured separately, but due to a lack of proper testing equipment, estimations of the vehicle properties had to be made. The following is a list of the values used to estimate the properties of the vehicle

- Vehicle mass ≈ 180 [kg]
- Wheel radius = 0.2032 [m]
- Gear ratio = 4:1
- Coefficient of rolling resistance ≈ 0.015
- Coefficient of static friction ≈ 0.025
- Coefficient of drag ≈ 0.5
- Area ≈ 0.7 m²
- Density of air ≈ 1.2 [kg-m⁻³]

D. Battery Model

The system uses 3-12V lead-acid batteries with a capacity of 44 Ah that were manufactured by Interstate. These were chosen by Phase I for their low cost and because this group was not concerned with power-to-weight ratio for this vehicle.

1. Model Development

In order to create an accurate representation of the voltage drop seen in the battery during large current draws, a model had to be developed that utilized voltage as a function of current drawn (A) and extracted capacity (Ah). Using the equation 19 from SimPowerSystems [5] of a discharging lead-acid battery, a model was developed using Simulink©.

$$E = E_0 - K*Q/(Q - i_t)*i(t) - K*Q/(Q-i_t)*i_t \quad (19)$$

Where E = Battery Voltage [V]

E_0 = Constant voltage [V]

K = Polarization constant [Ah^{-1}]

$i(t)$ = Low Frequency Current Dynamics [A]

i_t = Extracted capacity [Ah]

Q = Maximum battery capacity [Ah]

Neglecting the low frequency current dynamics and using the factory ratings of the batteries purchased gives values of:

$$E_0 = 36 [V]$$

$$K \approx 0.04 [Ah^{-1}]$$

$$Q = 44 [Ah]$$

The extracted battery capacity is derived, by integrating the battery current drawn over time, and multiplying by 1/3600 (sec) to obtain (Ah). These values give an equation of:

$$E = 36 - 0.04*44/(44 - it)*i(t) - 0.04*44/(44-i_t)*i_t \quad (20)$$

This is the equation used to develop the battery model seen in Figure 14.

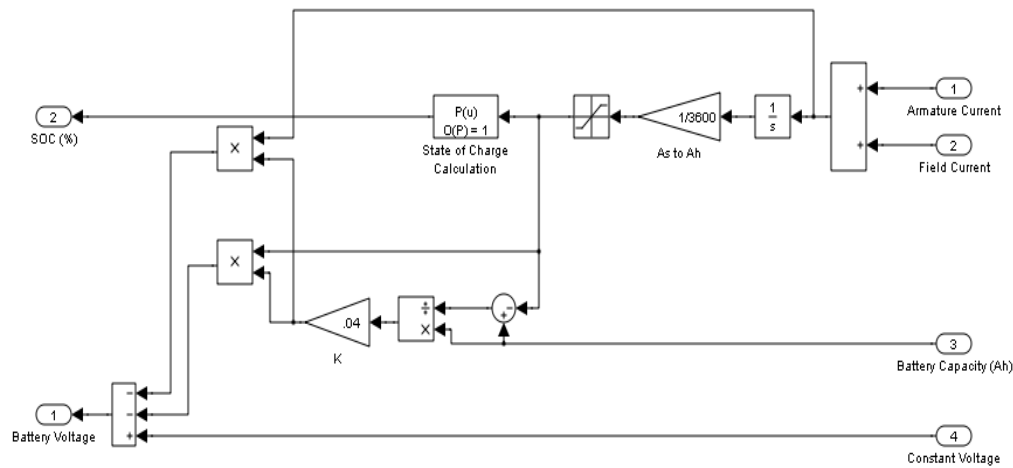


Figure 14: Simulink© Battery Model

2. Battery Model Results

A sample of the results from the theoretical battery model is shown in Figure 15. The input is a 100% throttle input for ten seconds. The current being drawn from the armature is saturated, in Simulink®, to 300 (A) to more accurately depict the realistic current draws of the motor. In the simulation, as the total battery current rises above 300 (A), there is a voltage drop of the battery, while the state of charge drops 1.5%. These values are untested, but do represent realistic predictions of the battery capabilities and is much more accurate than using an ideal voltage source in the vehicle model, which would allow for unrealistic torque developed by the motor.

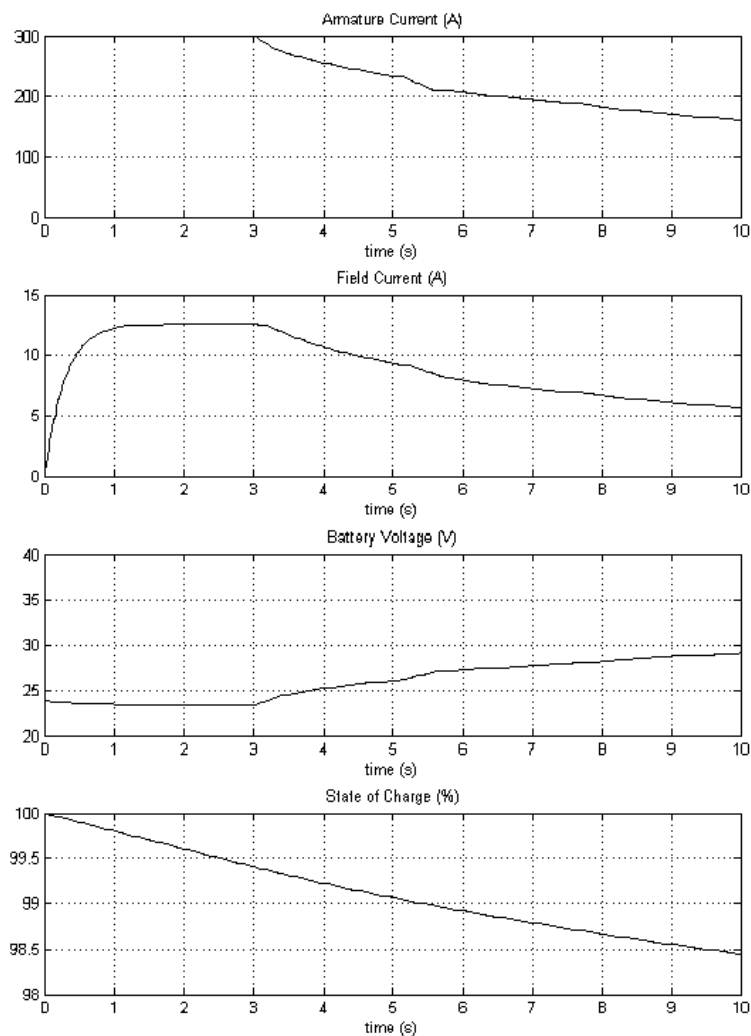


Figure 15: Battery Results

E. Complete System

The complete system model, which can be seen in Figure 16, is a compilation of all of the previous subsystems and acts as the vehicle as a whole. It utilizes a joystick input to control the throttle position and grade inputs, which are bound to the Y axis and slider of the joystick, respectively. There is also an input for passenger mass, which feeds into the vehicle dynamics subsystem. Various scopes can be attached to the outputs of each subsystem in order to observe individual characteristics and behaviors.

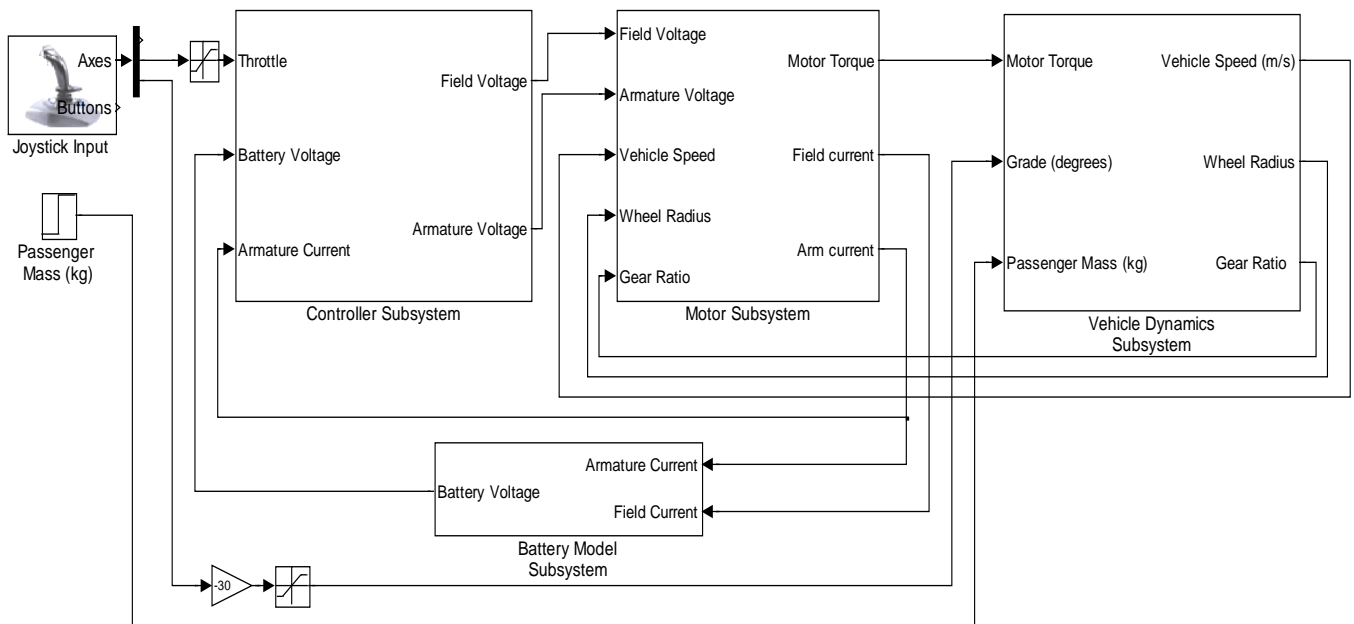


Figure 16: Simulink© Complete System Model

IV. Conclusion

In summary, the Phase II team has successfully developed motor, controller, vehicle dynamics and battery models. Through extensive testing and model development, an accurate motor model was developed, which was then also verified by comparing experimental data taken from the lab setup to the Simulink© model results. The controller model was derived through empirical techniques, which relate the inputs of throttle position and armature current to create outputs of armature and field voltage duty cycles. This model was made accurate at high motor loads by using the high speed dynamometer as described before. Like the motor model, the controller model's accuracy

has been verified by comparing experimental results to the results produced by Simulink©.

The Phase II team has also been successful in the development of a vehicle dynamics model and battery model. Due to the time constraint, it was impossible to experimentally test for all the parameters in these models and also verify the accuracy of these models. Although these models could not be verified experimentally, the results are reasonable given a general knowledge of battery and vehicle behaviors.

V. Recommendations for Future Work

Future teams of the MUEV project should begin with creating an accurate battery model that is tested and verified with the current batteries. Also, the Data Acquisition System (DAQ), which is referenced in appendix A, must be mounted on the vehicle platform in order to verify the vehicle dynamics and complete system model. In order to mount the DAQ, a portable voltage source must be used, as well as a new current sensor that can operate with a uni-polar voltage source. The DAQ will also need to be integrated with the digital tachometer on the tire to measure wheel RPM, which will be converted to speed. The armature and field voltages will need to be converted to a digital input so the sampling frequency can be increased, which will allow for a more accurate duty cycle reading. Also, the throttle position sensor must be integrated into the DAQ. It would also be helpful to more accurately measure the mass of the vehicle, as well as the load force coefficients.

As a more in-depth look at the model is required, it will be necessary to model the regenerative braking characteristics of the motor and controller and model auxiliary loads such as heat, air conditioning, lighting and radio. Finally, the components of the vehicle should be optimized. For example, the current batteries have a very limited capacity, and during testing on the dynamometer, would begin to fail after about 10-20 minutes. With the current vehicle model, a model of a lithium ion battery can be substituted into the battery model and the driving length of the vehicle can be calculated. The last stage of the project would be to design a zero carbon emissions charging station that will use photovoltaics to power the MUEV while at the owner's home.

VI. Patents

Table 7 lists a number of relevant patents for both phases of the MUEV design [4].

Table 7: Relevant Patents

Phase I Patents	
<i>Patent number</i>	<i>Description</i>
5,291,960	Hybrid electric vehicle regenerative braking energy recovery system
5,585,209	Bipolar lead/acid batteries
5,941,328	Electric vehicle with variable efficiency regenerative braking depending upon battery charge state.
6,037,751	Method and apparatus for charging batteries
6,116,368	Electric vehicle with battery regeneration dependent on battery charge state
6,866,350	Regenerative braking on an electrical vehicle when towed
7,455,133	Electric four-wheel drive vehicle and control unit for same
7,546,536	Electric motor
Phase II Patents	
<i>Patent number</i>	<i>Description</i>
5,878,189	Control system for a separately excited DC motor
6,192,745	Method and system for simulating vehicle and roadway interaction
6,885,951	Method and device for determining the state of function of an energy storage battery
7,098,665	Method for prediction of the internal resistance of an energy storage battery, and a monitoring device for energy storage batteries
7,498,772	Method and system of modeling energy flow for vehicle battery diagnostic monitoring

VII. Standards

U.S. Department of Energy – Illinois Electric Laws and Incentives:

Neighborhood Vehicle Access to Roadways

Neighborhood vehicles may only be operated on streets if authorized by the local government and where the posted speed limit is 35 miles per hour (mph) or less. Neighborhood vehicles are allowed to cross a road or street at an intersection where the road or street has a posted speed limit greater than 35 mph. Neighborhood vehicles are defined as self-propelled, electronically powered, four-wheeled motor vehicles (or a self-propelled, gasoline-powered four-wheeled motor vehicle with an engine displacement under 1,200 cubic centimeters) which are capable of attaining in one mile a speed of more than 20 mph, but not more than 25 mph, and which conform to federal regulations under Title 49 of the Code of Federal Regulations, Part 571.500. (Reference 625 [Illinois Compiled Statutes 5/11-1426.1](#))

Underwriters Laboratories:

Standard for Safety, *Electric Vehicle (EV) Charging System Equipment, UL 2202*

This Standard covers conductive and inductive charging system equipment intended to be supplied by a branch circuit of 600 volts or less for recharging the storage batteries in over-the-road EVs. In an inductive charging system, there is no direct metal-to-metal electrical connection between the charger and the vehicle. Instead, electrical power is passed through an electromagnetic field between the primary winding of a transformer, which is usually located off board the vehicle, to the secondary winding of the transformer which is usually located on board the vehicle. Conversely, in a conductive charging system, power is passed from the charger to the vehicle though direct metal-to-metal contact by way of a coupler or a plug and receptacle suitable for EV charging.

Standard for Safety, *Personnel Protection Systems for EV Supply Circuits, UL 2231*

This Standard covers devices and systems intended for use in accordance with the *National Electrical Code*® (*American National Standards Institute/National Fire Protection Association 70*), to reduce the risk of electric shock to the user from accessible parts, in grounded or isolated circuits for charging EVs.

Standard for Safety, *Plugs, Receptacles, and Couplers for EVs, UL 2251*

This Standard covers plugs, receptacles, vehicle inlets, and connectors rated up to 800 amperes and up to 600 volts ac or dc, intended for conductive connection systems, for use with EVs in accordance with the *National Electrical Code*® for either indoor or outdoor nonhazardous locations.

Society of Automotive Engineers:

Standard for Hybrid Electric Vehicle (HEV) & Electric Vehicle (EV) Terminology, SAE J1715_200802

This SAE Information Report contains definitions for electric vehicle terminology. It is intended that this document be a resource for those writing other electric vehicle documents, specifications, standards, or recommended practices. Hybrid electric vehicle terminology will be covered in future revisions of this document or as a separate document.

Vibration Testing of Electric Vehicle Batteries, SAE J2380_200903

This SAE Recommended Practice describes the vibration durability testing of a single battery (test unit) consisting of either an electric vehicle battery module or an electric vehicle battery pack. For statistical purposes, multiple samples would normally be subjected to such testing. Additionally, some test units may be subjected to life cycle testing (either after or during vibration testing) to determine the effects of vibration on battery life. Such life testing is not described in this procedure; SAE J2288 may be used for this purpose as applicable.

Recommended Practice for Performance Rating of Electric Vehicle Battery Modules, SAE J1798_200807

This SAE Recommended Practice provides for common test and verification methods to determine Electric Vehicle battery module performance. The document creates the necessary performance standards to determine (a) what the basic performance of EV battery modules is; and (b) whether battery modules meet minimum performance specification established by vehicle manufacturers or other purchasers. Specific values for these minimum performance specifications are not a part of this document.

Recommended Practice for Packaging of Electric Vehicle Battery Modules, SAE J1797_200806

This SAE Recommended Practice provides for common battery designs through the description of dimensions, termination, retention, venting system, and other features required in an electric vehicle application. The document does not provide for performance standards. Performance will be addressed by SAE J1798. This document does provide for guidelines in proper packaging of battery modules to meet performance criteria detailed in J1766.

U.S. Department of Transportation:

571.500 Standard No. 500; Low-speed Vehicles

571.305 Standard No. 305; Electric-powered vehicles: electrolyte spillage and electrical shock protection.

National Electric Code 2005 Edition:

Article 625 – Electric Vehicle Charging Systems

VIII. References

- [1]. Dieter, Kyle, Spencer Leeds, and Nate Mills. *Micro Urban Electric Vehicle & Test Platform*. Senior Project. Electrical and Computer Engineering Department, Bradley University. May 2009. <http://ee1.bradley.edu/projects/proj2009/move/index.html>
- [2]. M.H. Rashid, *Power Electronics - Circuits, Devices, and Applications*. Englewood Cliffs: Prentice-Hall Inc., 1988, pp. 296-300.
- [3]. Egeland, Olav, and Jan Gravdahl. "Modeling and Simulation for Automatic Control." Trondheim, Norway: Marine Cybernetics, 2002. Print.
- [4]. Gillespie, Thomas D. *Fundamentals of Vehicle Dynamics*. 1st ed. SAE International, 1992. Print.
- [5]. "SimPowerSystems - Battery." MathWorks, Web.
<<http://www.mathworks.com/access/helpdesk/help/toolbox/physmod/powersys/ref/battery.html>>.

Appendix A: Data Acquisition System

To develop the most accurate possible Simulink© models, many tests needed to be performed, in which several measurements needed to be taken and logged for later analysis. Also, these measurements needed to be highly accurate in order to model the subsystems of the Micro Urban Electric Vehicle effectively. To obtain these measurements, it was necessary to acquire a data acquisition system.

The main requirements for this system were for it to be easily mountable on the vehicle alongside a laptop to perform the task of displaying data in real time to the test driver while also logging the data for later use. This system also needed to be capable of measuring all of the signals necessary to develop and verify the accuracy of the mathematical models of the vehicle. The list of the measurements that were necessary for development of the Simulink© models is listed in Table A-1.

Table A-1: Measurement List

Measurement	Signal Type
Armature Voltage	Differential Voltage Signal
Armature Current	Analog Voltage Signal
Field Voltage	Differential Voltage Signal
Field Current	Analog Voltage Signal
Battery Voltage	Differential Voltage Signal
Battery Current	Analog Voltage Signal
Wheel Speed	Digital TTL Signal
Motor Temperature	Analog Voltage Signal
Battery Temperature	Analog Voltage Signal
Throttle Position	Analog Voltage Signal

To meet the requirements for data acquisition discussed above, a National Instruments device was purchased. Figure A-1 shows an image of the external hardware purchased for this application. It is a National Instruments CompactDAQ USB data acquisition system, which is specifically designed for applications similar to this project. This particular chassis is a four-slot design able to handle four unique modules that can accept the variety of signals described in Table A-1.



Figure A-1: Data Acquisition System

The four modules selected for this project were the following:

- NI 9215 4 channel 16-Bit, +/-10 V, 100 kS/s/ch, differential input measurement device
- NI 9221 8-Ch ± 60 V, 800 kS/s, 12-bit input module
- NI 9211 4-Ch ± 80 mV, 14 S/s, 24-Bit thermocouple and differential input module
- NI 9401 8-Channel, 100 ns, TTL digital input and output module.

These four modules have the capability to measure all of the signals listed in Table A-1.

To perform the signal manipulation and data logging for this application, the LabVIEW Full Development software was also purchased. The LabVIEW software allows the user to easily interact with the CompactDAQ in order to take and record measurements. Also, the LabVIEW software uses two interfaces (examples are shown on the following pages) in the development of a software program: the block diagram window and the front panel window. The block diagram page is used in the main development of the program. In this area, the programmer uses blocks that have predefined functions to perform the desired task for the user. The front panel window is an area that is designed for user interaction with the program that was designed in the block diagram window. Here, the user interacts with the program through the use of switches, buttons, waveforms and graphs, which are predefined by the developer of the program.

Using the LabVIEW software, a program was built to record data in a laboratory setting for this project (the final program is shown on the following pages). In the top left corner of the block diagram window is a block called “DAQ Assistant”, which represents the CompactDAQ hardware as described before. This block handles all of the signals coming into the laptop through the CompactDAQ. For this application, these signals include battery voltage, field voltage, armature voltage, field current, throttle position, and armature current, in this order. The signals are grouped into one data stream coming out of the DAQ Assistant block but are immediately split into their separate components for individual manipulation.

The battery voltage is read using the $\pm 60\text{V}$ analog input module and then is plotted to a waveform graph. As for the field and armature voltage measurements of the motor, it was necessary to use the $\pm 10\text{V}$ differential input module. However, the voltage signals of the field and armature are pulse width modulated signals with an amplitude of 36V . To overcome this problem, voltage division was used to divide these signals by four in order to read them through the $\pm 10\text{V}$ input. Then in software, both the field and armature voltages are multiplied by four to get back to the original signal. These two signals are plotted to waveform graphs and are then passed through a block, which takes the cycle average and finally displays the two average voltages of the motor. Note the armature voltage is measured from the M- to the B- terminal of the controller inverting

the duty cycle. Therefore, the armature voltage is subtracted from 36V to obtain the original signal.

In this lab setup, the field current was measured using a current-to-voltage transducer, which uses a Hall Effect sensor to produce a voltage proportional to the current passing through the transducer. The relationship between the voltage and current is linear, with the current being 12 times that of the voltage output of the transducer. The voltage from the transducer is measured using $\pm 10V$ differential input. This signal then becomes the field current, which is multiplied by 12 in software and then plotted on a waveform graph. Armature current of the motor is measured using a shunt that has a resistance of $0.1m\Omega$. This resistance creates a small voltage as current flows through the shunt, which is measured using the thermocouple input of the CompactDAQ. In software, this signal is multiplied by 1000 to get the corresponding armature current and is plotted to a waveform graph.

In this application, a $5k\Omega$ potentiometer was used to simulate the throttle position input. During testing, the throttle position was related to the voltage of the potentiometer by acquiring the voltage using a digital multimeter and the throttle position by using the controller data logged on the laptop. With this data set, a best fit technique was used to create a relationship between potentiometer voltage and throttle position. The relationship between the two is:

$$Y = 4.324469*X^2 + 25.015076*X - 2.218747 \quad (\text{A-1})$$

Where X is the voltage of the Potentiometer and Y is the throttle output as a percentage. Using the $\pm 10V$ differential input module, the voltage of the potentiometer was measured. In software, the signal is passed through a formula block that applies Equation A-1 shown above. The output of this equation is throttle position as a percentage, which is passed to a needle gauge and a waveform graph for user indication.

The final portion of this program merges all of the signals back together and re-samples them at a rate of 1Hz. Then the re-sampled signals are passed to a write to file block which, when enabled by the user, writes all of the signals to a file that can be opened using a spreadsheet program, such as Microsoft Excel. The same set of data is also written to a spreadsheet table in the front panel window to display real time data to the user.

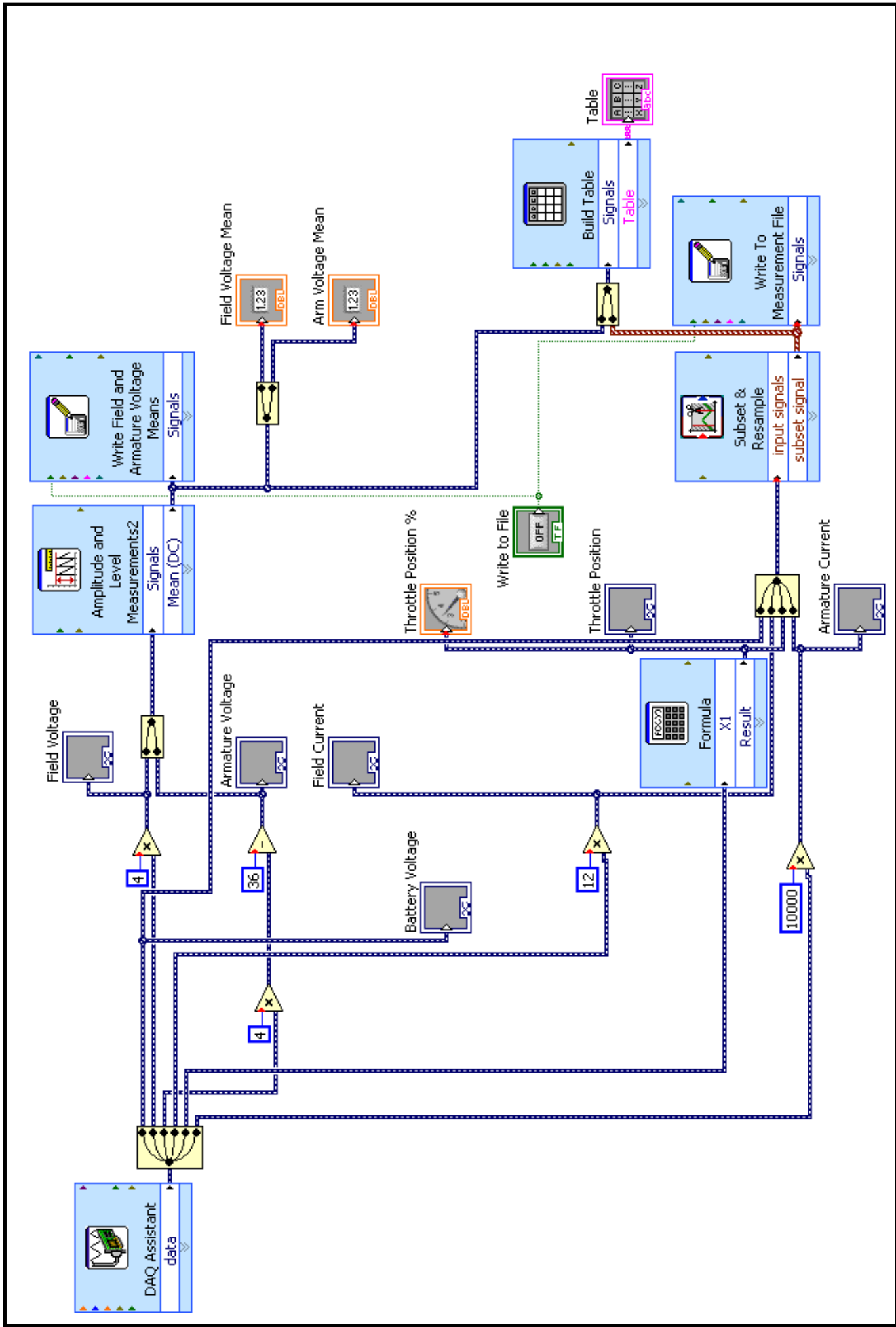


Figure A-2: Block Diagram Test Program

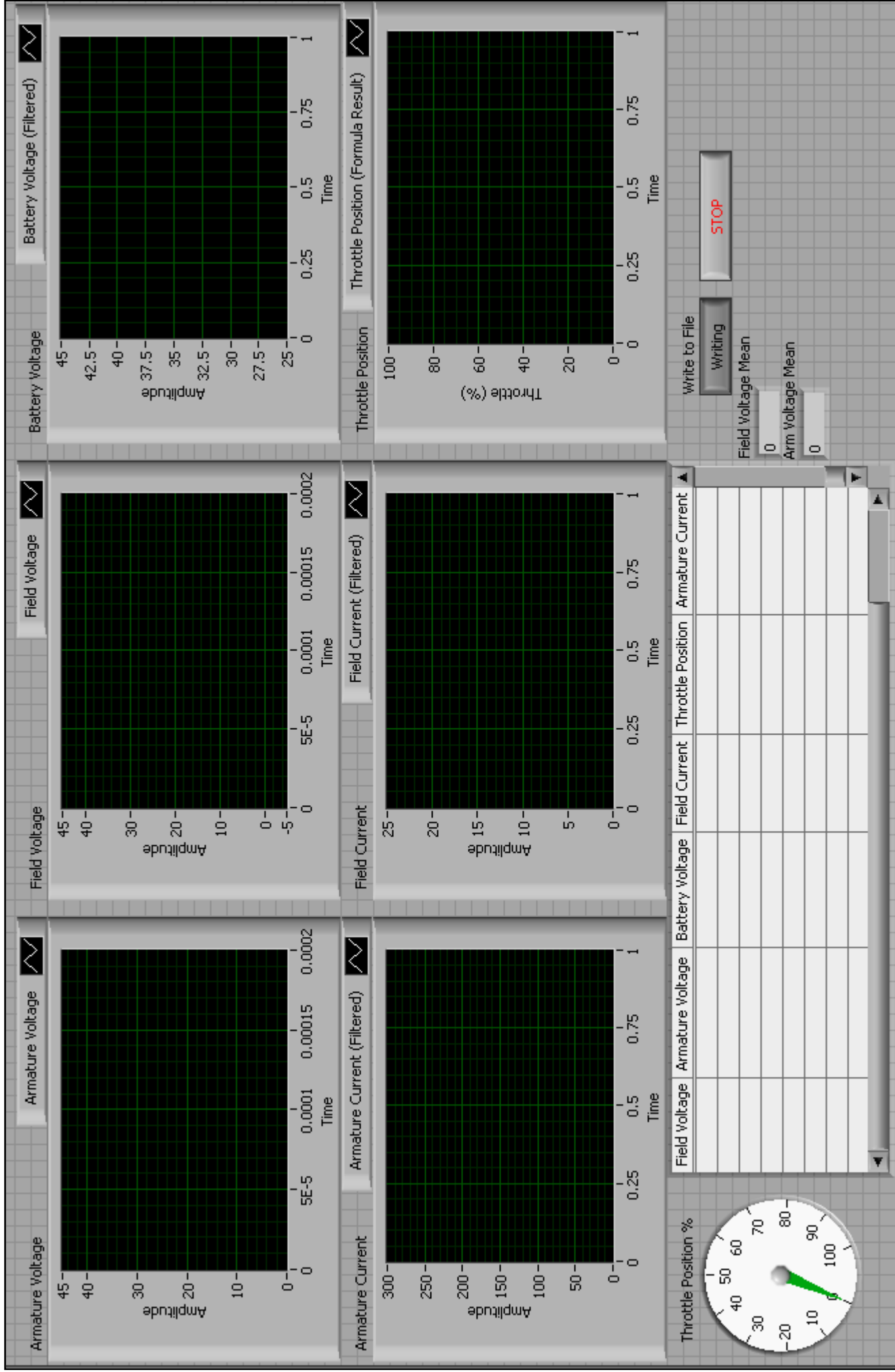


Figure A-3: Front Panel Test Program

Appendix B: Motor Test Data

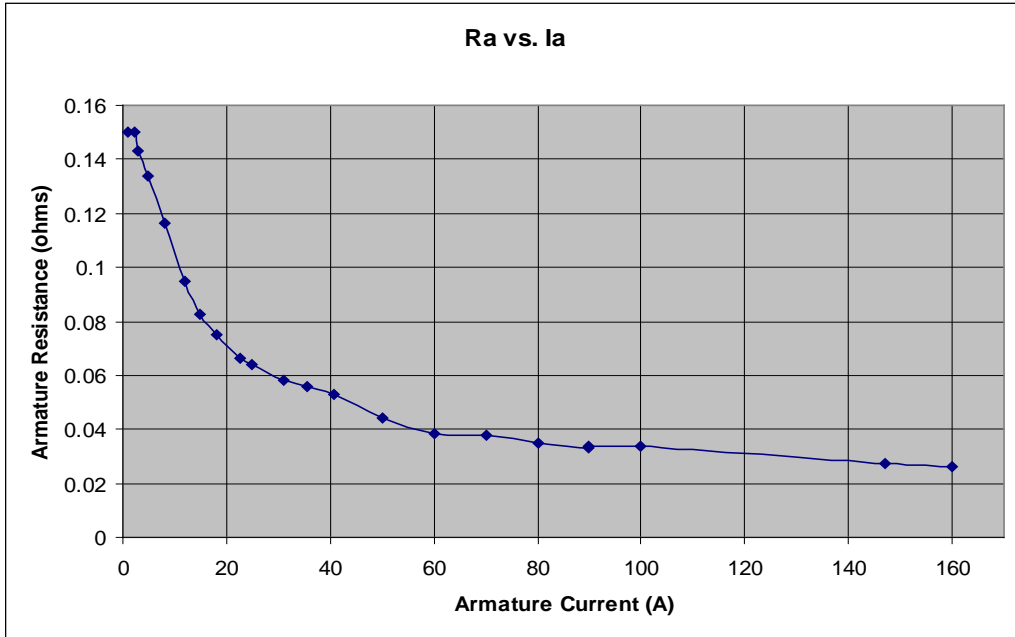


Figure B-1: Graph of Ra vs. Ia

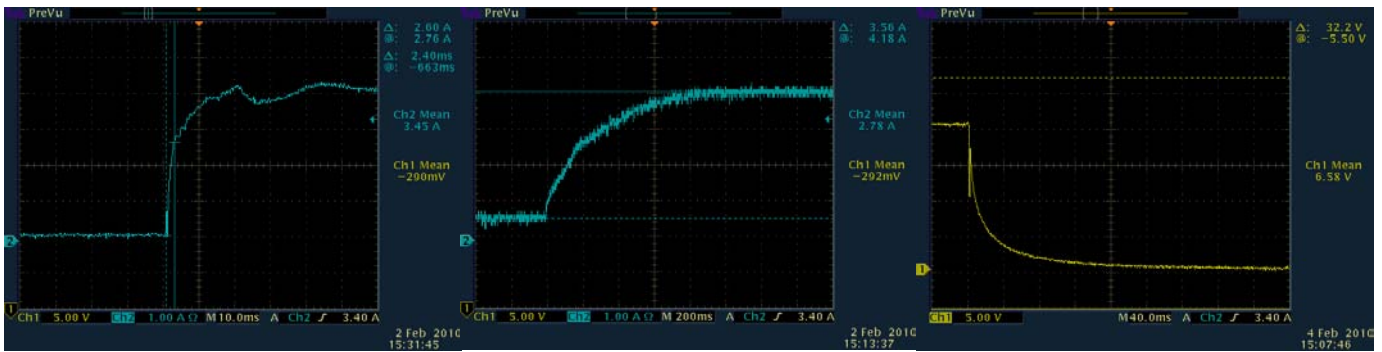


Figure B-2: L_a , L_f , J_m Transient Responses

Appendix C: Vehicle Dynamics Subsystems

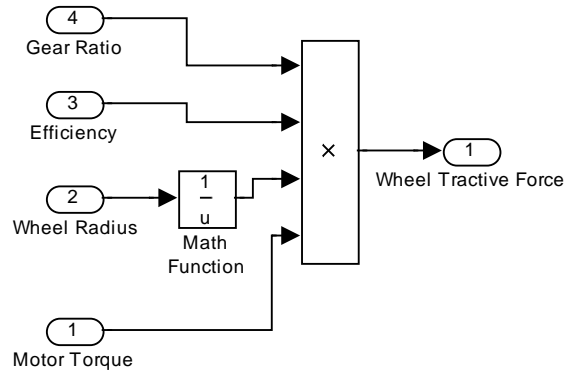


Figure C-1: Torque to Force Conversion Subsystem

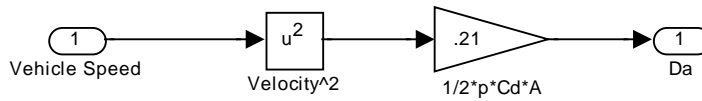


Figure C-2: Aerodynamic Force Subsystem

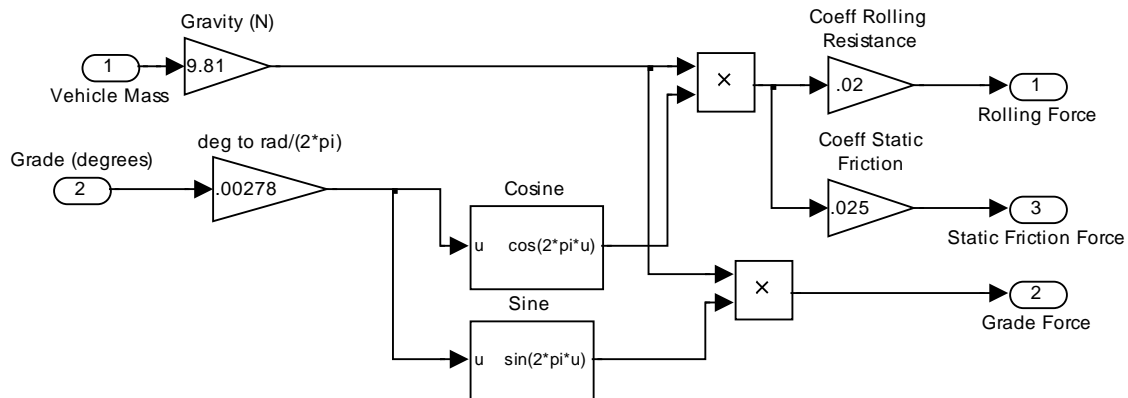


Figure C-3: Static Friction, Rolling Resistance and Grade Force Subsystem

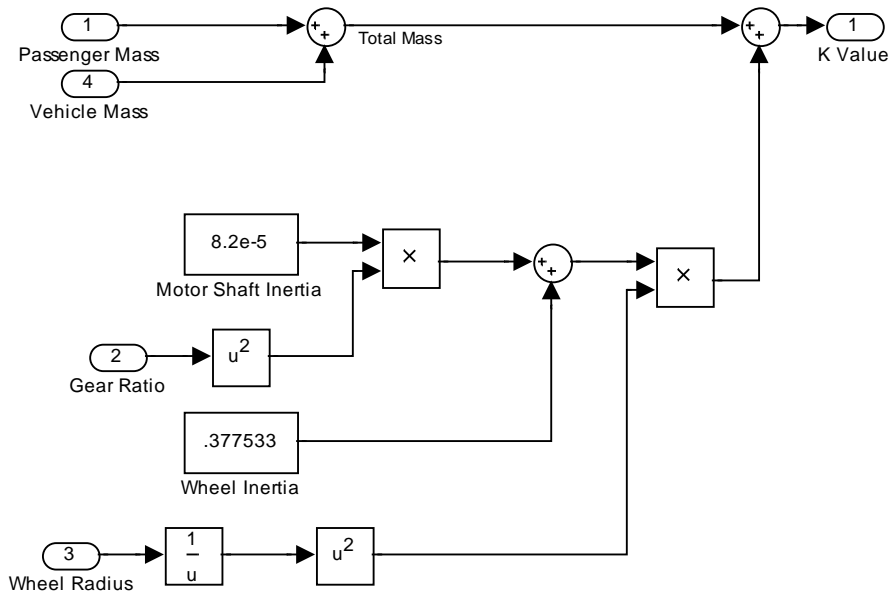


Figure C-4: Effective Translational and Rotational Mass